The final publication is available at

http://dx.doi.org/10.1021/acscatal.7b00778

Additional Information

Enhanced stability of Cu clusters of low atomicity against oxidation. The impact on catalytic redox process

Patricia Concepción,[1] Mercedes Boronat,[1] Saray García-García,[1] Estefanía Fernández,[1] Avelino Corma[1,2,*]

[1]Instituto de Tecnología Química, Universitat Politècnica de València-Consejo Superior de Investigaciones Científicas (UPV-CSIC), Av. de los Naranjos s/n, 46022 Valencia, Spain.

[2]King Fahd University of Petroleum and Minerals, P. O. Box 989, Dhahran 31261, Saudi Arabia.

ABSTRACT: By combining theoretical modelling, XPS and SERS spectroscopic studies, it has been found that it is possible to stabilize metallic copper species under oxidizing reaction conditions by adjusting the atomicity of sub-nanometer copper clusters. Small Cu_5 clusters display low reactivity toward O_2 dissociation, being less susceptible to be oxidized than larger Cu_8 or Cu_{20} systems. However, in the presence of water this reactivity is strongly enhanced, leading to oxidized Cu_5 clusters. In that case, the interaction of Cu_5 with atomic O oxygen is weak, favoring recombination and O_2 desorption, and suggesting an easier transfer of O atoms to other reactant molecules. In contrast, copper clusters of higher atomicity or nanoparticles, like Cu_8 or Cu_{20}, are easily oxidized in the presence of O_2 leading to very stable and less reactive O atoms, impairing a low reactivity and selectivity in many oxidation reactions. Altogether, Cu_5 clusters are proposed as promising catalyst for catalytic applications where stabilization of metallic copper species is strongly required.

KEYWORDS: clusters, DFT, XPS, Raman, catalysis, reactivity, electrochemical synthesis

INTRODUCTION

In the last decades, sub-nanometer transition metal clusters composed by a few atoms have attracted a great deal of attention because of their unique electronic, physical and chemical properties.[1] When the size of metal particles decreases to 1 nm or below, the electronic band structure of bulk metals changes to a discontinuous structure consisting of discrete electronic levels. This molecular-like electronic structure together with the low coordination and accessibility of all atoms in metal clusters give as a result an exceptional catalytic activity for many important reactions.[2] For instance, small Au clusters with less than 10 atoms have been identified as the catalytically active species in CO, alkane and thiol oxidation reactions,[2-6] and in C-C and C-heteroatom bond forming reactions,[7] sub-nanometer Pt clusters show enhanced activity in oxidative dehydrogenation of alkanes[8] and in the oxygen reduction reaction,[9] Ag_3 clusters supported on Al_2O_3 catalyze the epoxidation of propene with O_2 with high activity and selectivity at low temperature,[10] water stabilized Pd_3 and Pd_4 are highly active catalytic species in ligand free C-C cross-coupling reactions,[11] and a clear size-dependent CO oxidation activity has been reported for Pd clusters supported on TiO_2.[12] The scientific interest in the catalytic properties of copper clusters has increased in the last years, and some publications have appeared reporting improved catalytic performance of sub-nanometer Cu clusters in the chemoselective hydrogenation of carbonyl and olefin groups,[13] in the reduction of CO_2 to methanol with H_2,[14,15] the oxidation of CO with N_2O,[16] and in C-C, C-N, C-O, C-S and C-P bond forming reactions.[17]

Copper based catalysts have also been tested in oxidation reactions like CO oxidation and olefin epoxidation using molecular oxygen as oxidant, but the main drawback usually observed is a fast formation of copper oxides under reaction conditions, with the corresponding change in the catalytic properties. For instance, it has been reported that metallic copper exhibits a high selectivity to the epoxide in the partial oxidation of several olefins, but this selectivity drops when the catalyst surface becomes oxidized.[18-21] Linic et al, taking advantage of the light induced reduction of Cu atoms by photoexcitation of the localized surface plasmon resonance of Cu, succeeded in the stabilization of metal copper species under operating propene epoxidation conditions, improving this way the selectivity to propene epoxide from ☐20 to ☐50%.[21] In the case of CO oxidation it has been reported that copper catalysts deactivate under reaction conditions,[22] and although there is not full agreement about the nature of the most active copper oxidation state, either metallic copper[23,24] or Cu_2O,[25,26] it is generally accepted that formation of CuO deactivates the catalyst surface.[22]

It seems therefore really challenging to control the formation of Cu_2O and CuO oxide phases under reaction conditions, with the concomitant change in catalytic activity and selectivity. In this direction, in view of the possibility to tune the chemical properties of metal nanoparticles by adjusting particle size, and bearing in mind the completely different chemical and catalytic properties of metals in the sub-nanometer regime, one appealing approach, not yet reported, would be the possibility to stabilize metallic copper species by adjusting the atomici-

ty of copper clusters. We recently investigated by means of DFT calculations the dissociation of O_2 on Cu_n clusters and nanoparticles of increasing size, and a clear reactivity trend with cluster atomicity was found: i.e. calculated activation energies for O-O bond dissociation increase from less than 10 kcal/mol on small copper nanoparticles of ~1 nm diameter, to 15-20 kcal/mol on 3D clusters composed by 7-10 atoms, and to more than 40 kcal/mol on planar Cu_n clusters with n ≤ 5.[27] But that study focused only on the reactivity towards O_2 dissociation, not on the reverse process, and the question remains whether there is also a trend in the further reducibility of these copper clusters composed by a few atoms, which is key to stabilize metallic copper species and to produce efficient and long-lasting oxidation catalysts. In this sense, the present study focuses on the oxidizability and reducibility of copper clusters of low atomicity (5-20 atoms), where DFT results have been linked with experimental data obtained with laboratory scale cluster catalysts.

RESULTS AND DISCUSSION

DFT study. Using the optimized geometries reported in our previous DFT study,[27] the recombination of oxygen atoms adsorbed on the copper clusters to form molecular O_2 and its subsequent desorption leaving metallic clusters have been now analyzed, and the computed Gibbs free energies have been used to calculate equilibrium constants and kinetic constants for adsorption, dissociation and recombination processes. The optimized structures of reactant ($Cu_n - O_2$), transition state (TS) and product ($Cu_n - 2O$) of O_2 dissociation reaction over Cu_5, Cu_8 and Cu_{13} model clusters[27] are depicted in Figure 1 together with the corresponding Gibbs free energy profiles.

The oxidation of metallic clusters by reaction with molecular O_2 could be described by:

$$Cu_n + O_2 \xrightleftharpoons{K_{ads}} Cu_n - O_2 \xrightarrow{k_{dis}} Cu_n - 2O \quad (1)$$
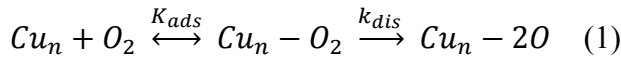
Where K_{ads} is the equilibrium constant for O_2 adsorption on the Cu_n clusters and k_{dis} is the kinetic constant for dissociation of the O-O bond in adsorbed O_2. They can be calculated as $K_{ads} = e^{\frac{-\Delta G_{ads}}{RT}}$, and $k_{dis} = \frac{k_B T}{h} e^{\frac{-\Delta G^{\ddagger}_{dis}}{RT}}$, respectively, with the Boltzmann constant k_B = 1,38065·10^{-23} J K^{-1} and the Planck constant h = 6,62607·10^{-34} J·s. From equation (1), the amount of dissociated $Cu_n - 2O$ species will depend on the product $K_{ads} \cdot k_{dis}$, whose variation with temperature is plotted in Figure 2, as well as that of k_{dis}.

As suggested by the activation free energy barriers, the kinetic k_{dis} constant and therefore the rate of O_2 dissociation increases with temperature and follows the order $Cu_{13} > Cu_8 > Cu_5$. But when O_2 adsorption is also taken into account, the difference between Cu_{13} and the smaller clusters widens, and the rate of oxidation of Cu_{13} becomes twenty orders of magnitude larger, (Figure 2a,b) a difference that should be clearly observable experimentally.

In a similar way, the reduction of the oxidized systems could be described by:

$$Cu_n - 2O \xrightarrow{k_{rec}} Cu_n - O_2 \xrightleftharpoons{K_{des}} Cu_n + O_2 \quad (2)$$
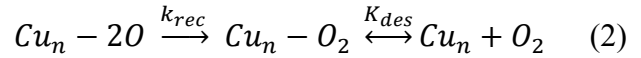
Where k_{rec} is the kinetic constant for recombination of two O atoms into adsorbed O2 and K_{des} is the equilibrium constant for O_2 desorption from the Cu_n clusters, and they can be calculated as $k_{rec} = \frac{k_B T}{h} e^{\frac{-\Delta G^{\ddagger}_{rec}}{RT}}$ and $K_{des} = e^{\frac{-\Delta G_{des}}{RT}}$, respectively. Notice that O_2 dissociation over Cu_5 causes a morphological change of the cluster from planar to 3D, and as a consequence a different pathway exists for the recombination step on Cu_5 (purple dotted lines in Figure 1b) that involves a lower Gibbs free activation energy barrier and produces a less stable adsorbed O_2 system. Again, the k_{rec} and $k_{rec} \cdot K_{des}$ calculated using the DFT Gibbs free energy values were plotted as a function of temperature (Figure 2c,d). While the trend in the kinetic constant k_{rec} for recombination of two O atoms over Cu_5 and Cu_{13} is not too different, when desorption of the formed O_2 molecule leaving the naked cluster is taken into account the global process is clearly favored on Cu_5 cluster, suggesting an easier reduction of the smallest copper clusters.
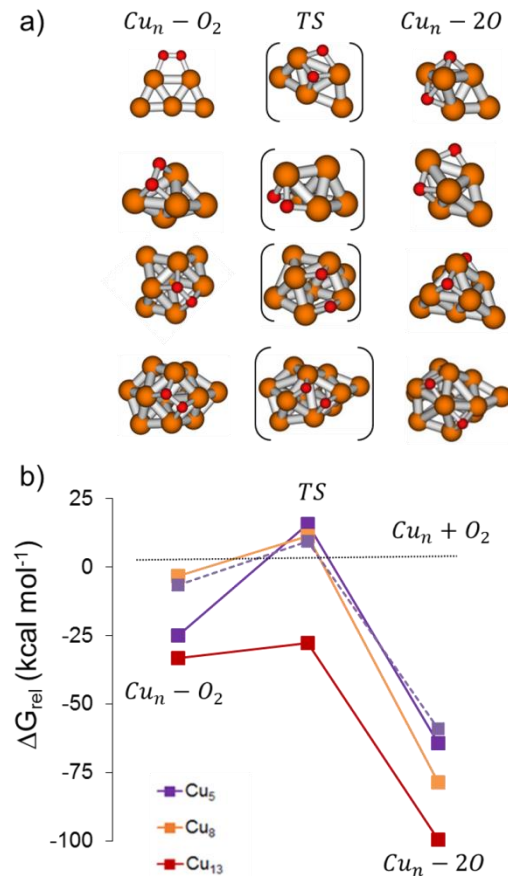
Figure 1. a) Optimized structures of reactant, transition state and product (from reference 27) and b) calculated Gibbs free energy profile for dissociation of molecular O_2 into two adsorbed O atoms over Cu_5 (purple), Cu_5-3D (purple, dashed lines),Cu_8 (orange) and Cu_{13} (red) clusters.
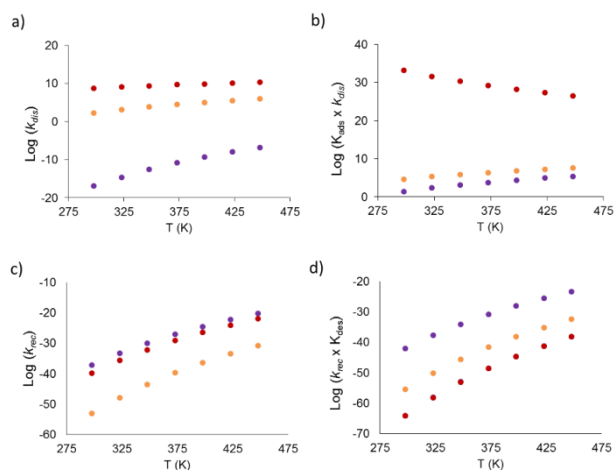
Figure 2. Logarithm of calculated kinetic and equilibrium constants for molecular O_2 dissociation and atomic O recombination as a function of temperature over Cu_5 (purple) Cu_8 (yellow) and Cu_{13} (red) clusters. a) kinetic constant for O_2 dissociation, k_{dis}, b) product of equilibrium constant for O_2 adsorption by k_{dis}, $K_{ads} \cdot k_{dis}$, c) kinetic constant for recombination of two O atoms forming adsorbed O_2, k_{rec}, and d) product of equilibrium constant for O_2 desorption by k_{rec}, $K_{des} \cdot k_{rec.}$

Finally, the strength of the interaction between copper clusters and atomic oxygen was measured by the interaction energy ΔG_{int} calculated as:

$$\Delta G_{int} = G(Cu_n - O) - G(Cu_n) - \frac{1}{2}G(O_2)$$

The values obtained, -25,1, -32,1 and -36,1 kcal·mol^{-1} for Cu_5, Cu_8 and Cu_{13} clusters respectively, are in line with the relative stability of the Cu_n – 2O systems shown in Figure 1, and suggest that the O atoms adsorbed on small clusters should be easier to transfer to other molecules than those adsorbed on larger three-dimensional copper clusters. Thus, the higher ability of copper clusters of increasing atomicity to be oxidized leading to a relatively stable copper oxide compound agrees with the observed catalytic behavior of conventional copper catalysts. In opposite to that behavior, we report high activation barriers for O_2 dissociation and an easier reduction of peroxidized Cu_5 clusters allowing stabilization of metallic copper under oxidizing reaction conditions. While the high energetic barrier for O_2 dissociation could hinder the global oxidation activity of Cu_5, the presence of other reactant molecules may modify the energetic profile and, accordingly, cluster reactivity.[28] For this reason the role of water on O_2 dissociation, which is present in many reactions as a reactant or as a product, has been evaluated and discussed below. Now, in order to confirm the trends arising from the DFT study, copper clusters of controlled atomicity have been synthesized in the laboratory scale and their oxidation-reduction behavior evaluated by means of surface sensitive spectroscopic tools.

Spectroscopic studies. The experimental confirmation of reactivity trends in the sub-nanometer regime is not an easy task, because it requires the synthesis of clusters within a very narrow size distribution and the use of non-

conventional and highly sensitive characterization techniques. Here, three samples of copper clusters composed by average cluster sizes of 5 (Cu_5), 8 (Cu_8), and 20 atoms (Cu_{20}), were synthesized electrochemically in the absence of stabilizing ligands following a previously reported method[29,30]. The as synthesized clusters were characterized by means of UV-VIS and photoluminescence techniques to determine their atomicity (see Figures S1-S3 in the Supporting Information).

Then, the trends in the ability of copper clusters and nanoparticles to activate O_2 and become oxidized, and to release oxygen and become reduced again closing the redox cycle were investigated by combining XPS and Surface Enhanced Raman Spectroscopy (SERS). XPS was used to determine the chemical state of the copper species, while SERS provides information about the interaction of copper samples with O_2. Prior to each study the Cu_5 and Cu_8 clusters were pre-activated in N_2 at 120°C to remove any adsorbed species remaining from the synthetic procedure. The evolution of the Cu $2p_{3/2}$ XPS core level binding energies (BE) and Cu L_3VV Auger electron kinetic energies (KE) of the Cu_5, Cu_8 and Cu_{20} samples, after having been exposed to controlled atmospheres (N_2 and O_2) in a high pressure reactor directly connected to the UHV-XPS analyzer chamber, are shown in Figure 3.
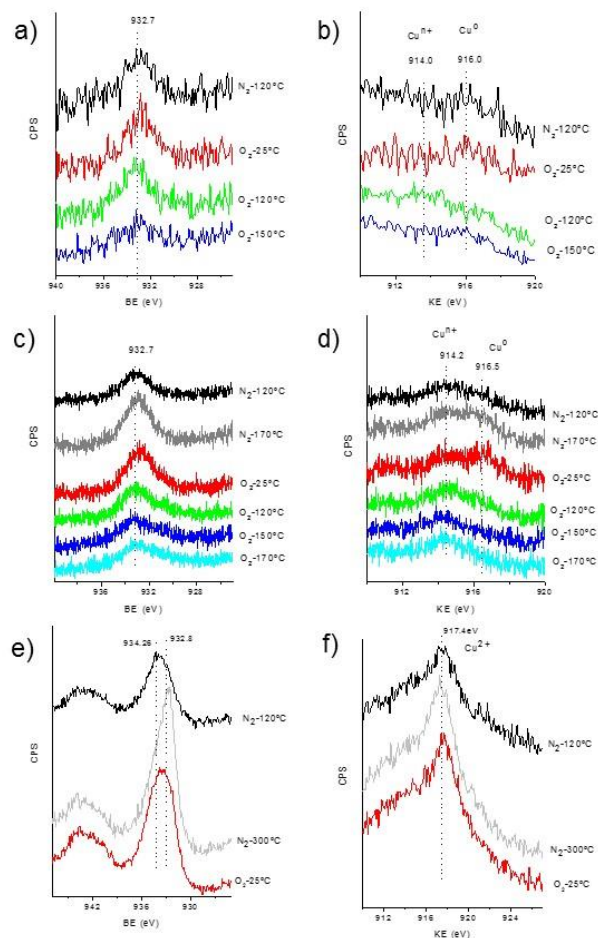

Figure 3. XPS study of Cu_5 (a-b), Cu_8 (c-d) and Cu_{20} (e-f) samples after N_2-O_2 treatments at different temperatures. a,c,e) Cu $2p_{3/2}$ XPS peak and b,d,f) CuL$_3$VV Auger peak.

With Cu_{20} sample, the BE value of 934.3 eV and the Cu L_3VV Auger peak at 917.5 eV correspond to Cu^{2+} ions in a CuO like structure. This oxidized state was stable under N_2 atmosphere up to a temperature of 250°C, and at 300°C Cu_{20} nanoparticles were partially reduced, as revealed by the growth of a new XPS component at a BE of 932.8 eV. After exposing the sample to molecular O_2, the peak at 932.6 eV decreased again in intensity due to a re-oxidation of the Cu_{20} clusters (Figure 3e,f).

In the case of Cu_5 and Cu_8 clusters and after pre-treatment in N_2 at 120°C, a similar Cu $2_{p3/2}$ BE peak at 932.7 eV was observed in the XPS spectra (Figure 3a,c), but different Cu L_3VV Auger kinetic energies were observed for the two systems, i.e. 916.0 eV for Cu_5 and 914.2 eV for Cu_8 (Figure 3b,d). After exposing the Cu_5 and Cu_8 clusters to N_2 and O_2 atmospheres, only modifications in the Cu L_3VV Auger electron kinetic energies (KE) were detected, due to the higher sensitivity to chemical environment effects of copper Auger peaks as compared to core level XPS values.[31,32] Indeed, when increasing temperature to 170°C in N_2, the Auger peak in the Cu_8 sample (Figure 3d, gray line) shifts from 914.2 eV to 916.5 eV, a value similar to that observed in the Cu_5 sample at 120°C in N_2. At this state, replacing N_2 with O_2 at a temperature of 25°C did not lead to any change in Cu_5 nor in Cu_8 samples (red spectra). When temperature rose to 120°C under O_2 atmosphere (green spectra), the initial Auger peak at 914.0 eV was partially observed in the Cu_5 sample, but it evolved again to the 916.0 eV peak with further increase of the temperature to 150°C in O_2 atmosphere (blue spectra). In the Cu_8 sample the 914.2 eV peak was restored at 120°C (green spectra), and it remained stable even after further increasing temperature to 150 and 170°C in the presence of O_2 (blue and cyan lines, respectively). Assignation of the observed KE values to a precise oxidation state of the copper species is difficult due to their anomalous values compared to conventional copper samples. This has been associated to initial and final state effects, particularly intra-atomic and extra-atomic relaxation energies of small clusters. Especially for metallic particles in the sub-nanometer range, the extra-atomic relaxation energy is strongly dependent on the size of the particle, and results in a shift of the KE to lower values at decreasing particle size.[33,34] Considering the shift of the Auger peak under the different atmospheres and comparing with the trends reported in the literature for copper compounds,[35-37] we can assign the peak at 914 eV to oxidized copper species, and the peak at 916 eV to copper species in a metallic state. In that case, the XPS studies would indicate a lower ability of Cu_5 clusters to interact with oxygen as compared to Cu_8 clusters, in agreement with the above reported DFT results.

To confirm this behavior, the nature of the Cu-O interaction in Cu_5 and Cu_8 samples under N_2 or O_2 atmospheres was followed by SERS spectroscopy (Figure 4). To assist in the assignment of the bands in the SERS spectra, the interaction of O atoms, O_2 and H_2O molecules, OH and OOH groups on Cu_5 and Cu_8 clusters was modelled by means of DFT calculations. The calculated vibrational frequencies have been organized according to the chemical system and the vibrational modes considered, and are summarized in Table 1.
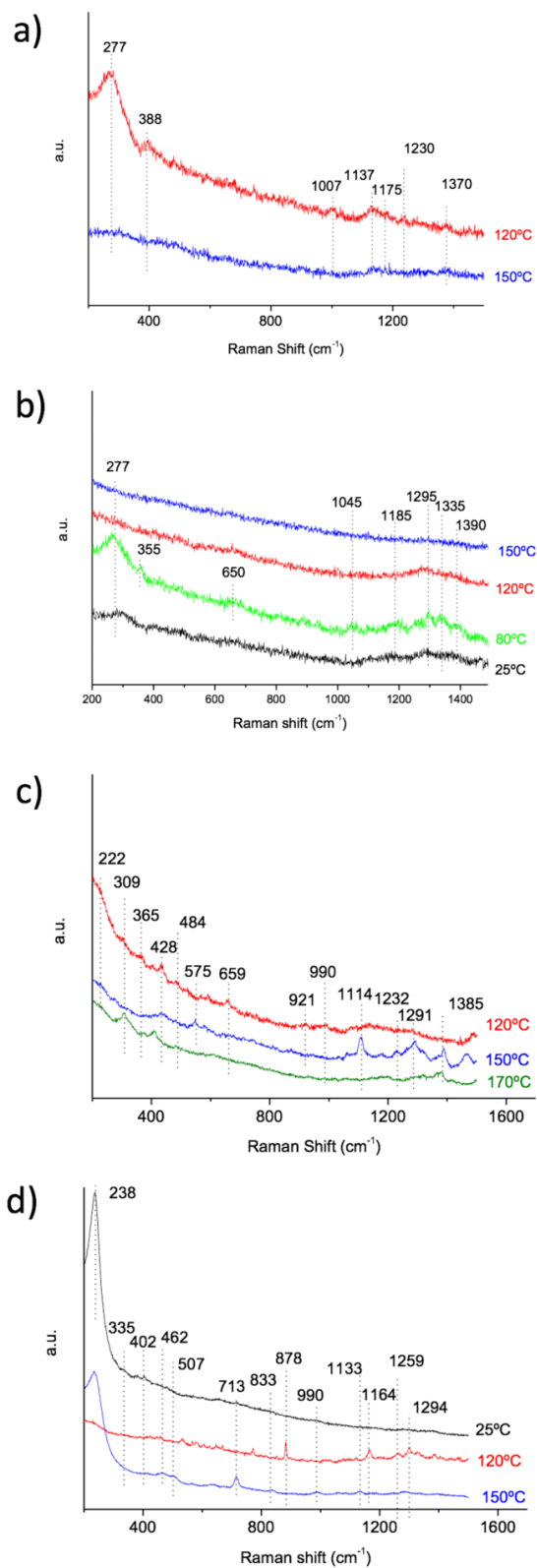

Figure 4. SERS spectra of Cu_5 (a,b) and Cu_8 (c,d) under N_2 flow at increasing temperatures (a,c) and after switching to O_2 flow at different temperatures (b,d).

Table 1. Calculated vibrational frequencies (in cm^{-1}) for selected vibrational modes in the adsorption complexes depicted in Figures S4-S7.

System	Vibrational mode	Cu$_5$	Cu$_8$
Cu$_n$ + O$_2$	O-O stretching		
	mono	1180 - 1440	
	bridge	1080 - 1260	1040 - 1130
	h-111	730 - 880	730 - 810
	Cu-O stretching		
	atomic O	300 - 670	300 - 650
	molecular O$_2$	220 - 580	240 - 570
Cu$_n$ + O$_2$ + H$_2$O	O-OH stretching		
	mono	1175	-
	bridge	780 - 870	780 - 850
	h-111	730 - 760	690 - 810
	O-OH bending		
	OOH	1190 - 1300	1160 - 1490
	Cu-O stretching		
	OOH or OH	330 - 510	340 - 530
	H$_2$O	240 - 360	220 - 350
	Cu-OH bending		
	OH	470 - 720	440 - 740

The main Raman bands in the Cu$_5$ sample after N$_2$ treatment at 120°C (Figure 4a, red line) appear in the 1035-1370 cm^{-1} frequency range, and are usually ascribed in the literature to different types of ν(O-O) stretching modes.[38,39] A signal at 270 cm^{-1} and a small peak at 388 cm^{-1}, which are in general related to Me-O stretching modes associated to atomic oxygen species and/or hydroxyl groups[40] were also observed. However, all these peaks were completely removed at 150°C under N$_2$ atmosphere (Figure 4a, blue line). Changing the gas flow from N$_2$ to O$_2$ at 25°C (Figure 4b, black line) resulted in the appearance of bands at 1045, 1185, 1295, 1335 and 1390 cm^{-1}, associated to the O-O bond stretching frequency in O$_2$ adsorbed in mono-coordinated or bridge conformations, and at 270 cm^{-1} which can be unambiguously ascribed to stretching of the Cu-O bond in molecularly adsorbed O$_2$. These bands were stable at 80°C, (Figure 4b, green line) but increasing the temperature to 120°C under O$_2$ flow caused a decrease in the intensity of all signals, which was especially visible in the disappearance of the 270 cm^{-1} band (Figure 4b, red line). Since XPS data pointed to a partial oxidation of the Cu$_5$ clusters at this stage, some O$_2$ dissociation may occur. In fact, two small Cu-O stretching signals at 355 and 650 cm^{-1}, corresponding to atomic O, were observed at 80°C (green line in Figure 4b). However, complete removal of all bands in the spectrum was observed at 150°C in the presence of O$_2$, indicating a weak Cu-O interaction that leads to O$_2$ desorption from metallic Cu$_5$ clusters. In the Raman spectra corresponding to Cu$_8$ sample, not only bands at high frequencies (1061, 1127, 1291 and 1430 cm^{-1}), but also lower frequency peaks ranging from 220 cm^{-1} to 922 cm^{-1} were observed under N$_2$ flow at 120°C and 150°C (red and blue lines in Figure 4c), which indicate the presence of atomic O. These bands decreased in intensity under N$_2$ flow at increasing temperatures, but they were not completely removed even at 170°C (Figure 4c, green line). By changing the N$_2$ flow to O$_2$ flow at 25°C, no change in the SERS spectra could be observed (Figure 4d, black line). However, when increasing the temperature to 120°C in the presence of O$_2$ flow, new bands in the 250-700 cm^{-1} frequency range started to appear (Figure 4d, red line) which, according to the DFT values reported in Table 1, are related to Cu-O stretching modes. These bands remained stable at 150°C, and confirm the higher stability of oxidized Cu$_8$ clusters as compared to Cu$_5$ clusters, in agreement with DFT and XPS results.

By combining the XPS and SERS data under the different atmospheres it is possible to conclude that Cu$_5$ clusters interact weakly with oxygen species, and are easier to reduce and more difficult to oxidize than Cu$_8$ sample. On the other hand, Cu$_{20}$ nanoparticles are less reducible, while they can be easily re-oxidized at 25°C. This picture is in full agreement with the results from the DFT study.

Role of water. As indicated above, the energy profile for O$_2$ dissociation can be modified due to the presence of other reactants or solvent molecules. For this reason, the possible role of water, which is present or generated in many reactions, has been investigated. The interaction of fully reduced Cu$_5$ clusters with pure water and with a mixture of water and O$_2$ was studied by SERS and XPS, and the complete reaction path for O$_2$ dissociation over Cu$_5$ clusters in the absence and presence of co-adsorbed water was theoretically investigated by means of DFT calculations.

Figure 5 shows the calculated Gibbs free energy profiles for dissociation of one molecule of O$_2$ over Cu$_5$ clusters in the absence (solid line) and presence (dashed line) of water, and the optimized geometries of the structures involved in these processes. As previously reported, molecular O$_2$ adsorbs in a bridge conformation over the most stable isomer of Cu$_5$ and dissociates with a high activation energy barrier of 40,7 kcal mol^{-1}, yielding a 3D cluster with two adsorbed O atoms (see Figure 1). Co-adsorption of a water molecule close to O$_2$ on planar Cu$_5$ facilitates the rupture of a copper-oxygen bond to produce, through transition state 2 with a free energy activation barrier as low as 6.0 kcal mol^{-1}, a system in which a hydrogen atom stabilizes the now mono-coordinated oxygen. It is easy from this point to generate co-adsorbed hydroxyl and hydroperoxyl groups (structure 5) in a process that involves a very low activation barrier of 2.7 kcal mol^{-1}. The mono-coordinated OOH group tends to form a more stable bi-coordinated fragment, thus causing a rearrangement of the copper atoms in the cluster which ultimately produces the highly stable structure 7 with an activation energy of only 4,3 kcal mol^{-1}. There is not a direct pathway for dissociation of the O-O bond in this system, but addition of a second water molecule yields

structure 8, with the H$_2$O molecule attached to the Cu atom in contact with the OOH ligand. A proton transfer from the adsorbed water to the OOH group breaks the O-O bond and generates intermediate 10 with an activation free energy barrier of 10.6 kcal mol^{-1}. Finally, water desorption leaves a Cu$_5$ cluster with two hydroxyl groups and one O atom, the three of them adsorbed in concatenated edge modes that deform the cluster to a planar square capped geometry. As clearly observed in the energy profile, the rate determining step in the global process is the dissociation of the O-O bond in structure 8 through transition state 9, with a calculated activation energy of only 10.6 kcal mol^{-1}, which is much lower as compared to the 40.7 kcal mol^{-1} obtained in the absence of water. The lowering of the barrier by 30 kcal mol^{-1} when water is present increases the calculated rate constant for O$_2$ dissociation k$_{dis}$ by 20 orders of magnitude. So, the presence of water in the reaction media would considerably enhance the ability of Cu$_5$ clusters to activate molecular O$_2$.
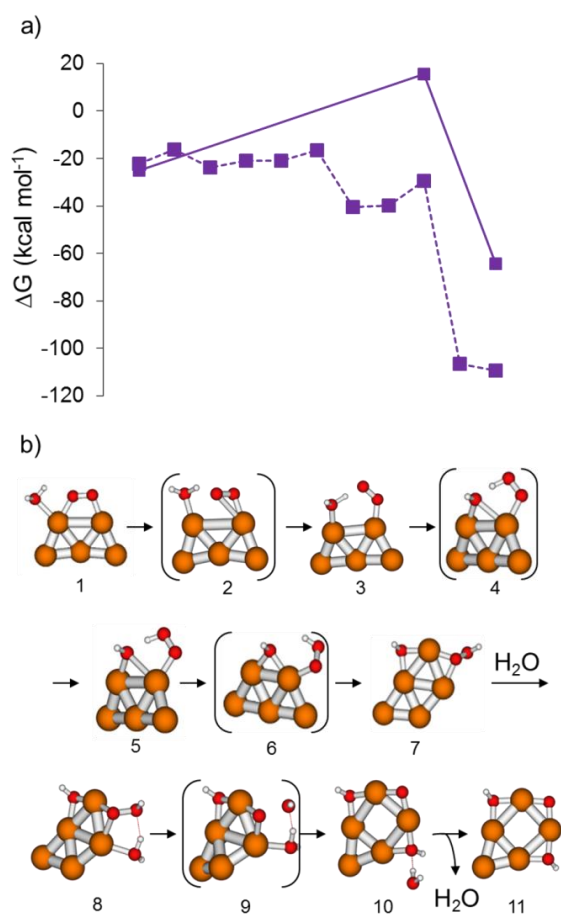

Figure 5. a) Calculated Gibbs free energy profiles for O$_2$ dissociation in the absence (solid lines) and presence (dashed and dotted lines) of water over Cu$_5$ clusters and b) optimized structures of all species involved in the water-assisted dissociation of O$_2$ over Cu$_5$ cluster.

To experimentally confirm this finding, the interaction of Cu$_5$ clusters in metallic state (after N$_2$ treatment at 120°C) with pure water and with a mixture of water and O$_2$ was studied by SERS and XPS spectroscopies (Figure

6). As discussed before, only bands associated to molecularly adsorbed O$_2$ were detected in the SERS spectra of Cu$_5$ under O$_2$ atmosphere at 25°C (see Figure 4b). In a similar experiment in the presence of only water (3wt% H$_2$O in N$_2$ flow) at 25°C, no bands were observed (see Figure 6c, black line), which demonstrates that Cu$_5$ clusters are not able to activate neither O$_2$ nor H$_2$O separately at 25°C. However, in the presence of a mixture of both O$_2$ and H$_2$O, (3wt% H$_2$O in O$_2$ flow) besides the bands at 255, 1087 and 1129 cm^{-1} corresponding to molecular O$_2$ adsorbed in a bridge conformation, several peaks at 399, 490, 546, 588, 655, 670 and 690 cm^{-1}, are clearly observed in Figure 6c, purple line. According to literature and to the data presented in Table 1, the peaks between 580 and 670 cm^{-1} are associated either to Cu-O stretching modes of atomic O or to bending modes of Cu-OH bonds, which demonstrate the promoting effect of water in dissociating O-O bonds.

As regards the reducibility of the partially oxidized system, it was found that increasing temperature to 120° and 150°C under N$_2$ atmosphere leads to complete desorption of all species, as already observed in previous experiments. Similar behavior could be deduced from the XPS spectra. As discussed before, after N$_2$ treatment at 120°C Cu$_5$ clusters appear in a metallic state which remains stable even after O$_2$ treatment at 25°C (Cu 2$_{p3/2}$ XPS BE of 932,7 eV and Cu L$_3$VV KE of 916.0 eV). In the presence of 3% water in O$_2$ flow a broadening of the Cu L$_3$VV peak toward higher KE (914.5 eV) could be observed, indicating the formation of oxidized copper species.
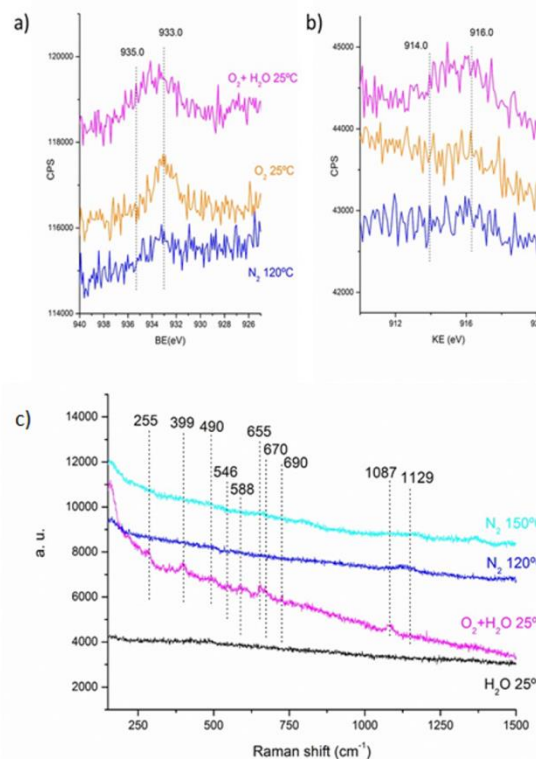

Figure 6. a) XPS spectra of fully reduced Cu$_5$ cluster after N$_2$ treatment at 120°C, followed by subsequent O$_2$ flow at 25°C

and 3%H_2O/O_2 flow at 25°C. a) Cu $2_{p3/2}$ XPS peak and b) CuL_3VV Auger peak. c) SERS spectra of fully reduced Cu_5 cluster (after N_2 treatment at 120°C) exposed to 3% H_2O/N_2 flow at 25°C, 3%H_2O/O_2 flow at 25°C, N_2 flow at 120°C and N_2 flow at 150°C.

In contrast with our finding that Cu_5 clusters are not able to dissociate H_2O in the absence of O_2, it has been recently shown that Cu clusters generated on a Cu(111) surface by means of CO adsorption are very active in dissociating water.[41] This apparent contradiction is explained by the different nature of Cu in the study by Eren et al., where the clusters are in fact defects associated to low-coordinated atoms on a metallic Cu surface, and in the present work, where isolated Cu_5 clusters dispersed on an inert support are investigated. Comparison of these two sets of results confirms the key role of the electronic structure of metal clusters of low atomicity in determining their catalytic properties.

CONCLUSIONS

According to the theoretical and experimental studies shown above, it seems possible to stabilize metallic copper clusters under oxidizing reaction conditions by adjusting the atomicity of the copper cluster. In that way, Cu_5 have shown low reactivity toward oxygen dissociation, being less susceptible to be oxidized. Thus Cu_5 clusters can be considered as very promising candidates for catalytic applications where stabilization of metallic copper species is strongly required. This is very appealing for practical applications in many oxidation reactions, like CO and CO_2 oxidation, cyclohexane and alkane oxidation, alcohol oxidation, propene epoxidation, etc., where copper overoxidation has been reported as responsible of their poor catalytic behavior. However the high activation energy required for oxygen activation on Cu_5 clusters could be detrimental for their catalytic performance. Fortunately, this can be overcome in the presence of water. Indeed, both theoretical and experimental data have shown that the reactivity of Cu_5 toward oxygen dissociation is strongly enhanced in the presence of water. The interaction of the resultant oxygen species with the copper cluster is weak, favoring oxygen recombination and O_2 desorption as well as a high reactivity of O atomic species with other reactant molecules. Altogether situate Cu_5 clusters as very promising catalysts for catalytic applications where oxidation of copper species has to be avoided. In contrast, copper clusters of higher atomicity, as for instance Cu_{20}, are highly susceptible to be oxidized in the presence of oxygen. The formed oxygen atoms are very stable resulting in a deep oxidation of the copper catalyst with the corresponding change in catalytic activity and selectivity.

EXPERIMENTAL SECTION

Electrochemical synthesis of copper clusters. Copper clusters were synthesized by an electrochemical procedure based on a modification of Reetz´s method.[42] In opposite to the synthesis procedure previously reported

by Quintela et al.,[29,30] ammonium salts were not used in our synthesis procedure. The synthesis was performed in a three electrode home-made electrochemical cell, working at room temperature and at 20 mA·cm^{-2}. Potassium nitrate (Sigma-Aldrich 99,0%) aqueous solution (0,1 M) was used as supporting electrolyte. A copper sheet (Goodfellow 99,9%) of 2 cm^2 was used as anode, while a platinum sheet (Goodfellow 99,95%) of the same size was used as cathode. As a reference electrode an Ag/AgCl system was employed. Both, the working electrode and de counter electrode were carefully cleaned before every synthesis.

During the electrochemical synthesis of copper clusters, the cell was maintained under nitrogen atmosphere and magnetic stirring. The obtained suspensions are composed of a brown solid and a colorless supernatant. The suspensions were purified by centrifugation (8000 rpm, 15 min) in order to separate the solid from the supernatant. Removing the supernatant, the solid was centrifuged again after dispersing in water (3x8000 rpm, 10 min) to eliminate the nitrate excess and the copper ions generated in the last stage of the synthesis. Finally, the obtained precipitate was re-dispersed in water and filtrated with a 0,45 μm membrane to isolate Cu_5 clusters. Cu_8 clusters were obtained starting from the Cu_5 solution, heating at 150 °C in a reflux system under N_2 atmosphere during 6h. Clusters of bigger size (Cu_{20}) were obtained after evaporation Cu_5 solution and subsequent re-dispersion in isopropanol. The concentration of the Cu_5 solution, determined by ICP, is c.a. 1 ppm. The atomicity of the copper clusters was determined according to UV-VIS and photoluminescence spectra.

Characterization methods.

Absorption spectra (200-800 nm) were performed using a Varian UV0811M209 spectrometer. The samples were placed in a 1 cm x 1 cm x 3 cm quartz cuvette, and the spectra acquired at 25°C.

Photoluminescence spectra (200-600 nm) were collected at room temperature using a Photon Technology International LP S-220B spectrometer and working with the same cuvettes as used in the adsorption studies.

XPS measurements. Photoelectron spectra were recorded using a SPECS spectrometer equipped with a 150MCD-9 Phoibos detector and using a MgKα (1253.6 eV) X-ray source. Spectra were recorded at -175°C and at 25°C, at grazing incident conditions (phi 5°), using an X-ray power of 50 W, an analyzer pass energy of 30 eV, and under an operating pressure of 10^{-9} mbar. Samples for XPS were prepared leaving a drop of the solution containing the clusters onto a quartz plate on which a N-doped graphene film was grown, fixed on a Mo sample holder, and by slowly evaporating the solvent in vacuum in the load lock of the XPS equipment. The growing of the N-doped graphene film onto the quartz plate was done according to ref. 43, and the choice of this material is based on a previous study[6] where the presence of N atoms in the organic support allows cluster stabilization. The chemical behavior of the clusters after having been exposed to controlled

atmospheres was studied in a reactor directly connected to the XPS equipment. After sample treatment at different gas flows, the samples were evacuated and directly transferred to the XPS analyzer chamber under vacuum. Under the working conditions no volatile Mo species are formed. Spectra treatment was performed using the CASA software.

Raman studies. Raman spectra were recorded with a 514 laser excitation on a Renishaw Raman spectrometer "In via" equipped with a CCD detector. The laser power on the sample was 15 mW and a total of 10 acquisitions were taken for each spectra. Due to the low intensity of the Raman signal as consequence of the low concentration of active species, spectra were acquired under SERS conditions (Surface Enhanced Raman Scaterring) using SERS "Randa" substrates supplied by AToID. SERS provides the same information traditionally provided by Raman spectroscopy, but with a significantly enhanced signal (of up to 10^4-10^6). It has been shown to be a very powerful technique in materials research due to its extremely high sensitivity permitting studies at very low surface coverage.[40] For analyzing the evolution of active species under controlled atmospheres, a commercial catalytic cell (http://www.linkam.co.uk/) was used allowing sample treatment at different temperatures and under different reactant flows, at a gas pressure of 1 atm. Raman data have only been used in a qualitative mode to identify species present, since quantification is not possible.

Computational details. All calculations in this work are based on density functional theory (DFT) and were carried out using the Gaussian 09 program package.[44] The hybrid B3PW91 functional, which combines the PW91 correlation functional by Perdew and Wang with the Becke's hybrid three-parameter exchange functional was employed.[45-47] Based on our previous study of copper clusters,[27] the Def2TZVP basis set, which constitutes a reformulation of the split-valence triple zeta basis set (TZVP) from Ahlrichs and co-workers,[48,49] was used for Cu atoms, while the standard 6-311+G(d,p) basis set by Pople was employed for O, C and H atoms.[50]

All structures involved in O_2 adsorption and dissociation in the absence of water were taken from ref. 27, while most of those used to assist in the assignment of Raman bands as well as those involved in the water-assisted mechanism were obtained in this work. In all cases, the positions of all atoms in the system were fully optimized without any restriction, and all stationary points were characterized by pertinent frequency analysis calculations. The frequencies obtained for all minima were further corrected with a scaling factor of 0.9656, as suggested by Andrade et al.[51] Transition states were determined through potential energy surface (PES) scans along with the subsequent optimizations and vibrational frequency calculations. Atomic charges and molecular orbital distributions were calculated using the natural bond order (NBO) approach.[52]

ASSOCIATED CONTENT

Supporting Information. UV/Vis and photoluminescence spectra of electrochemically synthesized copper clusters, and optimized structures of the systems used to calculate the vibrational frequencies listed in Table 1. This material is available free of charge via the Internet at http://pubs.acs.org.

AUTHOR INFORMATION

Corresponding Author

*acorma@itq.upv.es

Author Contributions

The manuscript was written through contributions of all authors.

REFERENCES

(1) Tyo, E. C.; Vajda, S. *Nat. Nanotechnol.* **2015**, *10*, 577-588.

(2) Boronat, M.; Leyva-Perez, A.; Corma A. *Acc. Chem. Res.* **2014**, *47*, 834-844.

(3) Yoon, B.; Hakkinen, H.; Landman, U.; Worz, A. S.; Antonietti, J. M.; Abbet, S.; Judai, K.; Heiz, U. *Science* **2005**, *307*, 403-407.

(4) Herzing, A. A.; Kiely, C. J.; Carley, A. F.; Landon, P.; Hutchings, G. J. *Science* **2008**, *321*, 1331–1332.

(5) Liu, Y.; Tsunoyama, H.; Akita, T.; Xie, S.; Tsukuda, T. *ACS Catal.* **2011**, *1*, 2–6.

(6) Corma, A.; Concepción, P.; Boronat, M.; Sabater, M. J.; Navas, J.; Yacaman, M. J.; Larios, E.; Posadas, A.; López-Quintela, M. A.; Buceta, D.; Mendoza, E.; Guilera, G.; Mayoral, A. *Nat. Chem.* **2013**, *5*, 775–781.

(7) Oliver-Meseguer, J., Leyva-Perez, A.; Corma, A. *ChemCatChem* **2013**, *5*, 3509-3515.

(8) Vajda, S.; Pellin, M. J.; Greeley, J.; Marshall, C. L.; Curtiss, L. A.; Ballentine, G. A.; Elam, J. W.; Catillon-Mucherie, S.; Redfern, P. C.; Mehmood, F.; Zapol, P. *Nat. Mat.* **2009**, *8*, 213–216.

(9) Yamamoto, K.; Imaoka, T.; Chun, W. J.; Enoki, O.; Katoh, H.; Takenaga, M.; Sonoi, A. *Nat. Chem.* **2009**, *1*, 397–402.

(10) Lei, L.; Mehmood, F.; Lee, S.; Greeley, J.; Lee, B.; Seifert, S.; Winans, R. E.; Elam, J. W.; Meyer, R. J.; Redfern, P. C.; Teschner, D.; Schlögl, R.; Pellin, M. J.; Curtiss, L. A.; Vajda, S. *Science* **2010**, *328*, 224–228.

(11) Leyva-Perez, A.; Oliver-Meseguer, J. Rubio-Marques, P.; Corma, A. *Angew. Chem., Int. Ed.* **2013**, *52*, 11554-11559.

(12) Kaden, W. E.; Wu, T.; Kunkel, W.A.; Anderson, S. L. *Science* **2009**, *326*, 826–829.

(13) Maity, P.; Yamazoe, S.; Tsukuda, T. *ACS Catal.* **2013**, *3*, 182–185.

(14) Vidal, A. B.; Feria, L.; Evans, J.; Takahashi, Y.; Liu, P.; Nakamura, K.; Illas, F.; Rodriguez, J. A. *J. Phys. Chem. Lett.* **2012**, *3*, 2275–2280.

(15) Liu, C.; Yang, B.; Tyo, E.; Seifert, S.; Debartolo, J.; von Issendorff, B.; Zapol, P.; Vajda, S.; Curtiss, L. A. *J. Am. Chem. Soc.* **2015**, *137*, 8676–8679.

(16) Hirabayashi, S.; Ichihashi, M. *Phys. Chem. Chem. Phys.* **2014**, *16*, 26500-26505.

(17) Oliver-Messeguer J.; Liu L.C.; Garcia-Garcia S.; Canos-Gimenez C.; Dominguez I.; Gavara R.; Domenech-Carbo A.; Concepcion P.; Leyva-Perez A.; Corma A. *J. Am. Chem. Soc.*, **2015**, *137*, 3894-3900.

(18) Cropley, Rachael L.; Williams, Federico J.; Urquhart, Andrew J.; Vaughan, Owain P. H.; Tikhov, Mintcho S.; Lambert, Richard M. *J. Am. Chem. Soc*. **2005**, *127*, 6069-6076.

(19) Torres, D.; Lopez, N.; Illas, F.; Lambert, R. M. *Angew. Chem., Int. Ed*. **2007**, *46*, 2055-2058.

(20) Greiner, M. T.; Jones, T. E.; Johnson, B. E.; Rocha, T. C. R.; Wang, Z. J.; Armbüster, M.; Willinger, M.; Knop-Gericke, A.; Shlögl, R. *Phys. Chem. Chem. Phys.* **2015**, *17*, 25073-25089.

(21) Marimuthu, A.; Zhang, J.; Linic, S.; *Science*, **2013**, *339*, 1590-1593.

(22) Royer, S.; Duprez, D. *ChemCatChem* **2011**, 3, 24–65.

(23) Jernigan, G. G.; Somorjai, G. A. *J. Catal*. **1994**, *147*, 567–577.

(24) Xu, F.; Mudiyanselage, K.; Baber, A. E.; Soldemo, M.; Weissenrieder, J.; White, M. G.; Stacchiola, D. J. *J. Phys. Chem. C* **2014**, *118*, 15902-15909.

(25) Sadykov, V. A.; Tikhov, S. F.; Bulgakov, N. N.; Gerasev, A. P. *Catal. Today* **2009**, *144*, 324–333.

(26) Eren, B.; Heine, Ch.; Bluhm, H.; Somorjai, G. A.; Salmeron, M. *J. Am. Chem. Soc*. **2015**, *137*, 11186–11190.

(27) Fernández, E.; Boronat, M.; Corma, A. *J. Phys. Chem. C* **2015**, *119*, 19832-19846.

(28) Hibbits, D.; Iglesia, E. *Acc. Chem. Res.* **2015**, *48*, 1254–1262.

(29) Vilar-Vidal, N.; Blanco, M.C.; López-Quintela, M.A.; Rivas, J.; Serra, C. *J. Phys. Chem. C* **2010**, *114*, 15924-15930.

(30) Vilar-Vidal, N.; Rivas, J.; López-Quintela, M.A.; *ACS Catal.* **2012**, *2*, 1693-1697.

(31) Grünert, W.; Hayes, N.W.; Joyner, R.W.; Shpiro, E.S.; Siddiqui, M.R.H.; Baeva, G.N. *J. Phys. Chem.* **1994**, *98*, 10832-10846.

(32) Vennestron, P.N.R.; Katerinopoulou, A.; Tiruvalam, R.R.; Kustov, A.; Moses, P.G.; Concepcion, P.; Corma, A. *ACS Catal.* **2013**, *3*, 2158-2161.

(33) Espinós, J.P.; Morales, J.; Barranco, A.; Caballero, A.; Holgado, J.P.; Gonzalez-Elipe, A.R.; *J. Phys. Chem. B* **2003**, *106*, 6921-6929.

(34) Morales, J.; Espinós, J.P.; Caballero, A.; Gonzalez-Elipe, A.R.; Mejias, J.A. *J. Phys. Chem. B* **2005**, *109*, 7758-7765.

(35) Briggs. D.; Seah, M.P. In Practical Surface Analysis by Auger and X-Ray Photoelectron Spectroscopy; John Wiley & Sons: New York, 1985.

(36) Moretti, G.; Fierro, G.; Lo Jacono, M.; Porta, P. S*urf. Interface. Anal.* **1989**, *14*, 325-336.

(37) Grünert, W.; Hayes, N.W.; Joyner, R.W.; Shpiro, E.S.; Siddiqui, M.R.H.; Baeva, G.N. *J. Phys. Chem.* **1994**, *98*, 10832-10846.

(38) Choi, Y.M.; Abernathy, H.; Chen, H-T.; Lin, M.C.; Liu, M. *Chem. Phys. Chem.* **2006**, *7*, 1957-1963.

(39) Root, D.E.; Mahroof-Tahir, M.; Karlin, K.D.; Solomon, E.I. *Inorg. Chem.* **1998**, *37(19)* 4838-4848.

(40) Niaura, G. *Electrochim.Acta.* **2000**, *45*, 3507-3519.

(41) Eren, B.; Zherebetskyy, D.; Patera, L. L.; Wu, C. H.; Bluhm, H.; Africh, C.; Wang, L. W.; Somorjai, G. A.; Salmeron, M. *Science* **2016**, *351*, 475-478.

(42) Reetz, M.T.; Helbig, W. *J. Am. Chem. Soc.* **1994**, *116*, 7401-7402.

(43) Primo, A.; Atienzar, P.; Sanchez, E.; Delgado, J. M.; García, H. *Chem. Commun.* **2012**, *48*, 9254-9256.

(44) Gaussian 09, Revision C.01, M. J. Frisch, G. W. Trucks, H. B. Schlegel, G. E. Scuseria, M. A. Robb, J. R. Cheeseman, G. Scalmani, V. Barone, G. A. Petersson, H. Nakatsuji, X. Li, M. Caricato, A. Marenich, J. Bloino, B. G. Janesko, R. Gomperts, B. Mennucci, H. P. Hratchian, J. V. Ortiz, A. F. Izmaylov, J. L. Sonnenberg, D. Williams-Young, F. Ding, F. Lipparini, F. Egidi, J. Goings, B. Peng, A. Petrone, T. Henderson, D. Ranasinghe, V. G. Zakrzewski, J. Gao, N. Rega, G. Zheng, W. Liang, M. Hada, M. Ehara, K. Toyota, R. Fukuda, J. Hasegawa, M. Ishida, T. Nakajima, Y. Honda, O. Kitao, H. Nakai, T. Vreven, K. Throssell, J. A. Montgomery, Jr., J. E. Peralta, F. Ogliaro, M. Bearpark, J. J. Heyd, E. Brothers, K. N. Kudin, V. N. Staroverov, T. Keith, R. Kobayashi, J. Normand, K. Raghavachari, A. Rendell, J. C. Burant, S. S. Iyengar, J. Tomasi, M. Cossi, J. M. Millam, M. Klene, C. Adamo, R. Cammi, J. W. Ochterski, R. L. Martin, K. Morokuma, O. Farkas, J. B. Foresman, and D. J. Fox, Gaussian, Inc., Wallingford CT, 2009.

(45) Perdew, J. P.; Chevary, J. A.; Vosko, S. H.; Jackson, K. A.; Pederson, M. R.; Singh, D. J.; Fiolhais, C. *Phys. Rev. B* **1992**, *46*, 6671–6687.

(46) Perdew, J. P.; Wang, Y. *Phys. Rev. B* **1992**, *45*, 13244–13249.

(47) Becke, A. D. *J. Chem. Phys.* **1993**, *98*, 5648–5652.

(48) Weigend, F.; Ahlrichs, R. *Phys. Chem. Chem. Phys.* **2005**, *7*, 3297–3305.

(49) Weigend, F. *Phys. Chem. Chem. Phys.* **2006**, *8*, 1057–1065.

(50) Binkley, J. S.; Pople, J. A.; Hehre, W. J. *J. Am. Chem. Soc.* **1980**, *102*, 939–947.

(51) Andrade, S. G.; Goncalves, L. C. S.; Jorge, F. E. *Journal of Molecular Structure-Theochem* **2008**, *864*, 20-25.

(52) Reed, A. E.; Weinstock, R. B.; Weinhold, F. *J. Chem. Phys.* **1985**, *83*, 735–747.